nature materials

LETTERS

PUBLISHED ONLINE: 18 APRIL 2010 | DOI: 10.1038/NMAT2747

A single-layer wide-angle negative-index metamaterial at visible frequencies

Stanley P. Burgos[1†], Rene de Waele[2†], Albert Polman[2] and Harry A. Atwater[1*]

Metamaterials are materials with artificial electromagnetic properties defined by their sub-wavelength structure rather than their chemical composition. Negative-index materials (NIMs) are a special class of metamaterials characterized by an effective negative index that gives rise to such unusual wave behaviour as backwards phase propagation and negative refraction. These extraordinary properties lead to many interesting functions such as sub-diffraction imaging[1,2] and invisibility cloaking[3–6]. So far, NIMs have been realized through layering of resonant structures, such as split-ring resonators, and have been demonstrated at microwave[7,8] to infrared[9–13] frequencies over a narrow range of angles-of-incidence and polarization. However, resonant-element NIM designs suffer from the limitations of not being scalable to operate at visible frequencies because of intrinsic fabrication limitations[14], require multiple functional layers to achieve strong scattering[13,14] and have refractive indices that are highly dependent on angle of incidence and polarization. Here we report a metamaterial composed of a single layer of coupled plasmonic coaxial waveguides that exhibits an effective refractive index of −2 in the blue spectral region with a figure-of-merit larger than 8. The resulting NIM refractive index is insensitive to both polarization and angle-of-incidence over a ±50° angular range, yielding a wide-angle NIM at visible frequencies.

Negative-index materials were first predicted theoretically by Veselago[15] in 1968, but it was only a decade ago that Pendry[16] defined NIM designs suitable for experimental realization. In these resonant-element based NIMs, the unusual 'left handed' behaviour of light originates from subwavelength resonant elements that behave like 'artificial atoms' with engineered diamagnetic resonances that are the source of the material's negative-index response. As such, NIMs were first demonstrated experimentally with arrays of millimetre-size copper strips and split-ring resonators operating at microwave frequencies[16,17]. This discovery sparked a considerable effort to scale down the size of the constituent resonant components to enable operation at higher frequencies. As a result, micrometre-size structures have been successfully fabricated to produce negative refractive indices at terahertz frequencies. More recently, NIMs have been fabricated to operate in the near-infrared spectral region. However, for operation at optical frequencies the required size of sub wavelength scatterers is very close to practical fabrication limits. So far, the highest reported operational frequency of NIMs has been demonstrated at the deep-red side of the visible spectrum ($\lambda_0 = 780$ nm) using 'fishnet' structures with features as small as 8 nm (ref. 14). Moreover, to achieve strong scattering, the material was built up from a stack of multiple physical layers—thus complicating the fabrication of resonant-element based NIMs for operation at visible frequencies.

Recently, using waveguides, a conceptually different approach was taken to achieve a negative refractive index in the optical spectral range. Investigation of the mode structure of two-dimensional metal/insulator/metal (MIM) plasmonic slab waveguides[18,19] reveals that certain MIM waveguide geometries support negative-index modes at visible frequencies. Arrays of such negative-index MIM slab waveguides can serve as a quasi three-dimensional metamaterial[20]. However, the negative-index mode in MIM waveguides[18] can only be excited from free space with the perpendicular polarization and off-normal angles of incidence because of the polarization and symmetry of the mode, respectively.

These practical limitations of planar MIM geometries can be circumvented in a coaxial MIM geometry in which the planar MIM waveguide is wrapped onto itself (Fig. 1). Similar to the modes supported by planar MIM plasmonic waveguides, the coaxial waveguide geometry is found to also support field symmetric and anti-symmetric modes that correspond to positive- and negative-index modes, respectively. However, unlike planar MIM waveguides, calculations of individual MIM plasmonic coaxial waveguides show a negative-index mode that, owing to the cylindrical symmetry of the structure, is accessible from free space independent of both incidence angle and polarization. Here, we demonstrate that a two-dimensional array of vertically oriented MIM coaxial waveguides, arranged in a dense hexagonal configuration, functions as a single-layer wide-angle negative index material down to the blue part of the visible spectrum. Through parameter retrieval analysis, we verify the NIM to have a double-negative[21] index band in the 450–500 nm spectral range. Furthermore, we find that the effective refractive index of this geometry is insensitive to both polarization and angle of incidence up to ±50°. Unlike the wire arrays of Liu *et al.*, which exhibit negative refraction but not a negative index[22], the coupled coaxial waveguide array exhibits a true negative refractive index characterized by negative refraction and backwards phase propagation.

Figure 1a schematically depicts the NIM, consisting of a hexagonal close-packed array of Ag/GaP/Ag MIM coaxial waveguides composed of 25 nm GaP annular channels with a 75 nm inner diameter set at a pitch of $p = 165$ nm in a Ag layer. We study the metamaterial response both by analytic waveguide modal analysis for single coaxial structures, and using finite-difference time-domain (FDTD) simulations for the array of coupled coaxial waveguides.

To estimate the effective refractive index of the material, we first calculate the mode index dispersion of the constituent coaxial elements by solving Maxwell's equations in cylindrical coordinates[23,24] for a single MIM coaxial waveguide of infinite length. The waveguide eigenmodes are characterized by a complex propagation constant along the z axis $\beta(\omega) = \beta'(\omega) + i\beta''(\omega)$, where β' and β'' are the real and imaginary parts of the propagation

[1]Kavli Nanoscience Institute, California Institute of Technology, MS 128-95, Pasadena, California 91125, USA, [2]Center for Nanophotonics, FOM Institute AMOLF, Science Park 104, 1098 XG Amsterdam, The Netherlands. †These authors contributed equally to this work. *e-mail: haa@caltech.edu.

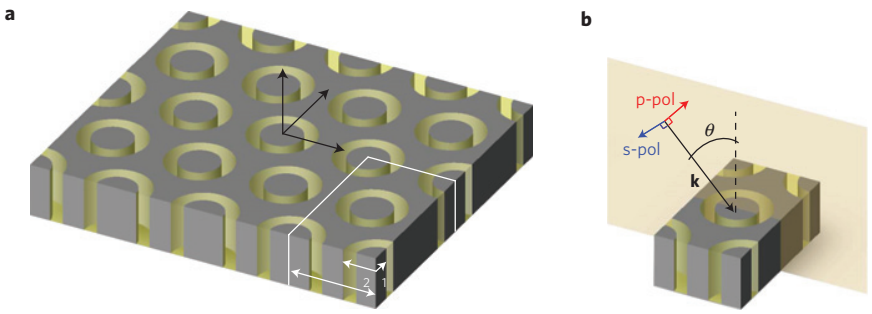

Figure 1 | Negative-index metamaterial geometry. a, Single-layer NIM slab consisting of a hexagonal array of subwavelength coaxial waveguide structures. The inner radius $_1$, outer radius $_2$ and array pitch are defined in the image. **b**, Unit cell of the periodic structure. The angle-of-incidence θ is shown, as well as the in-plane (p-) and out-of-plane (s-) polarization directions associated with the incident wavevector **k**.

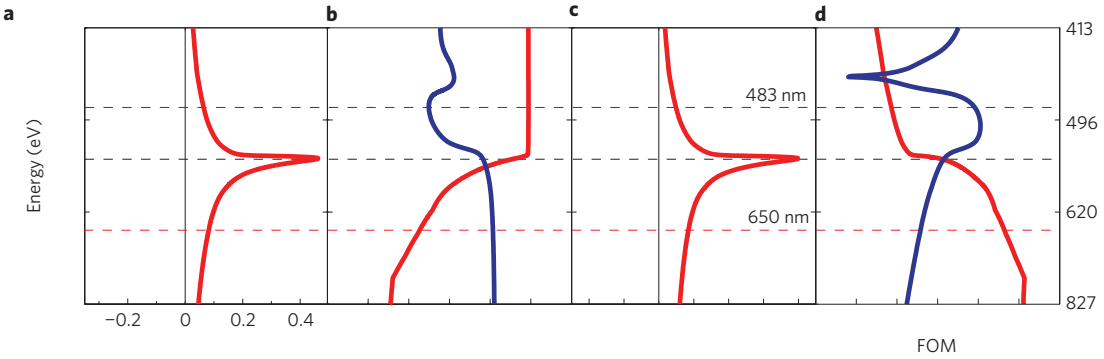

Figure 2 | Coaxial waveguide dispersion relations. The coaxial waveguide consists of an infinitely long 25 nm GaP annular channel with a 75 nm inner diameter embedded in Ag. Plotted are the two lowest order linearly polarized modes that most strongly couple to free space radiation. **a**–**c**, Energy is plotted versus β' (**a**), β'' (**b**) and mode index $_{\text{mode}}$ (**c**). **d**, The figure-of-merit FOM $= |\beta'/\beta''|$. The Ag/GaP planar surface plasmon energy at $\bar{}\omega_{SP} = 2.3$ eV ($\lambda_0 = 540$ nm) is indicated by the black dashed horizontal line. All panels show one mode with positive index (red curve) and one mode with a negative index (blue curve) below an energy of 2.7 eV ($\lambda_0 = 460$ nm). The insets in **a** show the Re( ) (out-of-page) field distribution in the waveguide at a wavelength of $\lambda_0 = 650$ nm for the positive-index mode and at $\lambda_0 = 483$ nm for the negative-index mode.

constant, respectively. Complex optical constants for Ag (ref. 25) and GaP (ref. 26) are taken from tabulated literature data.

Figure 2a and b show the calculated dispersion relations $\omega(\beta')$ and $\omega(\beta'')$ of a single Ag/GaP/Ag coaxial waveguide. The mode index $n_{\text{mode}} = c\beta'/\omega$ is plotted in Fig. 2c. Similar to what is reported for planar MIM structures[18] we find one mode with a positive index over the entire spectral range (red curve), and a second mode with a negative index for energies below 2.7 eV (blue curve). The index of the second mode ranges from $-9 < n_{\text{mode}} < 1$ in the energy range of Fig. 2. The insets in Fig. 2a show the Re(H_y) field profiles corresponding to the positive-index mode at $\lambda_0 = 650$ nm ($n_{\text{mode}} = 8.5$) and the negative-index mode at $\lambda_0 = 483$ nm ($n_{\text{mode}} = -2.0$). A full field map of the negative-index mode can be found in Supplementary Fig. S1. Figure 2b shows that for energies below $\hbar\omega_{SP} = 2.3$ eV the positive-index mode (red curve) has the lowest attenuation and will therefore be dominant, whereas for energies above $\hbar\omega_{SP}$ the negative-index mode (blue curve) is dominant. Figure 2d shows the figure-of-merit, FOM $= |\beta'/\beta''|$ (ref. 27), of the two modes. The lowest attenuation constant β'' for the negative-index mode is found at $\lambda_0 = 483$ nm, with a corresponding FOM of 8.3.

Next, we analyse the collective response of the coupled coaxial waveguide array using the FDTD method. Figure 3a shows a time-snapshot of Re(H_y) inside a 165 nm pitch coaxial waveguide array illuminated by a $\lambda_0 = 483$ nm p-polarized plane wave incident at 30°. At this pitch the waveguides are separated by 40 nm, corresponding to twice the radial skin depth ($\delta \sim 20$ nm) of an isolated coaxial waveguide mode into the Ag cladding. Phase fronts are observed to clearly refract in the negative direction, that is, to the same side of the interface normal. By following the phase fronts in time (Supplementary Movie S1) we observe backward phase propagation at an angle of −12.5° with respect to the interface normal, as indicated in Fig. 3a by the blue arrow labelled **k**.

Using Snell's law and the wavevector refraction angle inside the material, we find that the metamaterial has an effective refractive index of $n_{\text{eff}} = -2.3$, close to the mode index found for an individual coaxial waveguide at this wavelength ($n_{\text{mode}} = -2.0$). Furthermore, the direction of energy flow **S** inside the NIM layer, depicted by the green arrow in Fig. 3a, is found to be antiparallel to the phase velocity—a signature of a true negative index material. Thus, at a separation of 40 nm, the waveguides are coupled just enough to allow both power and phase to refract negatively across the waveguide structures with antiparallel directions, while only perturbing the metamaterial's effective index from that of a single coax by $\Delta n = -0.3$. From the wavelength in the metamaterial and the exponential energy decay in the waveguides we find a metamaterial FOM of 8, equal to the FOM calculated for isolated coaxial structures.

By repeating this analysis for angles ranging from 10° to 50°, for both s- and p-polarized light at $\lambda_0 = 483$ nm, we find very similar results for the material's response, with n_{eff} varying between −2.1 and −2.4. The data for p-polarized light are summarized in Supplementary Fig. S2. Such a small dependence of the index on polarization and angle-of-incidence has not been demonstrated in any other NIM reported so far. For example, Valentine *et al.* investigated only normal incidence excitation for a NIM operational in the near-infrared spectral region[12], whereas the negative-index mode in planar MIM structures can only be excited at off-normal

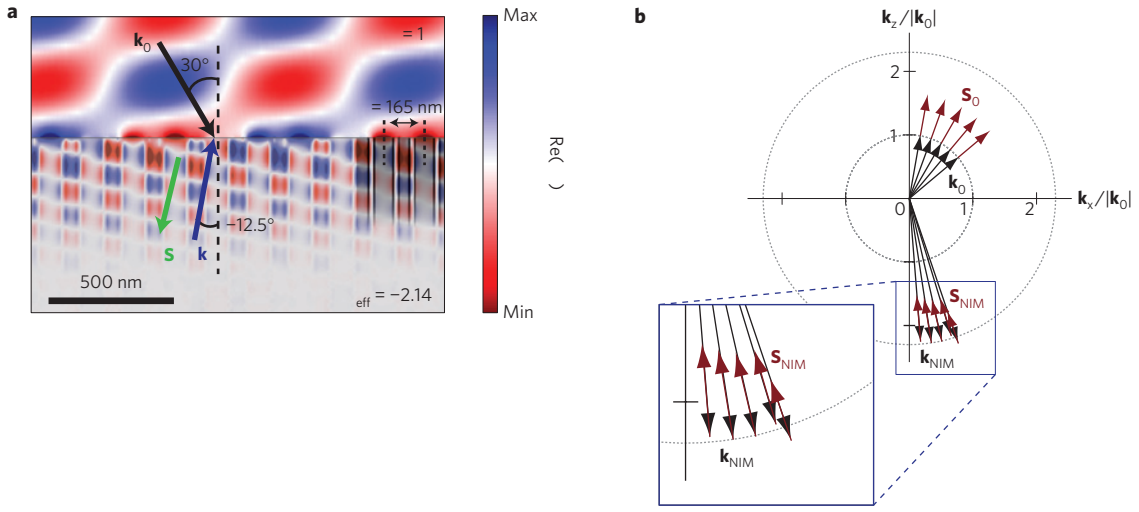

Figure 3 | Metamaterial index. a, Light at $\lambda_0 = 483$ nm is incident on a semi-infinite slab of single-layer negative index metamaterial at an angle of 30° from air. Shown is a time-snapshot of the magnetic field distribution Re( ) taken along the polarization plane. Arrows denote the direction of energy flow **S** and phase velocity **k**. The coax centre-to-centre pitch is schematically indicated. **b**, Constant-frequency surface plot at $\lambda_0 = 483$ nm showing the relation between **k** and **k** for a semi-infinite metamaterial slab over a 50° range of incidence angles. The wavevector **k** and Poynting vector **S** data are derived from FDTD simulations.

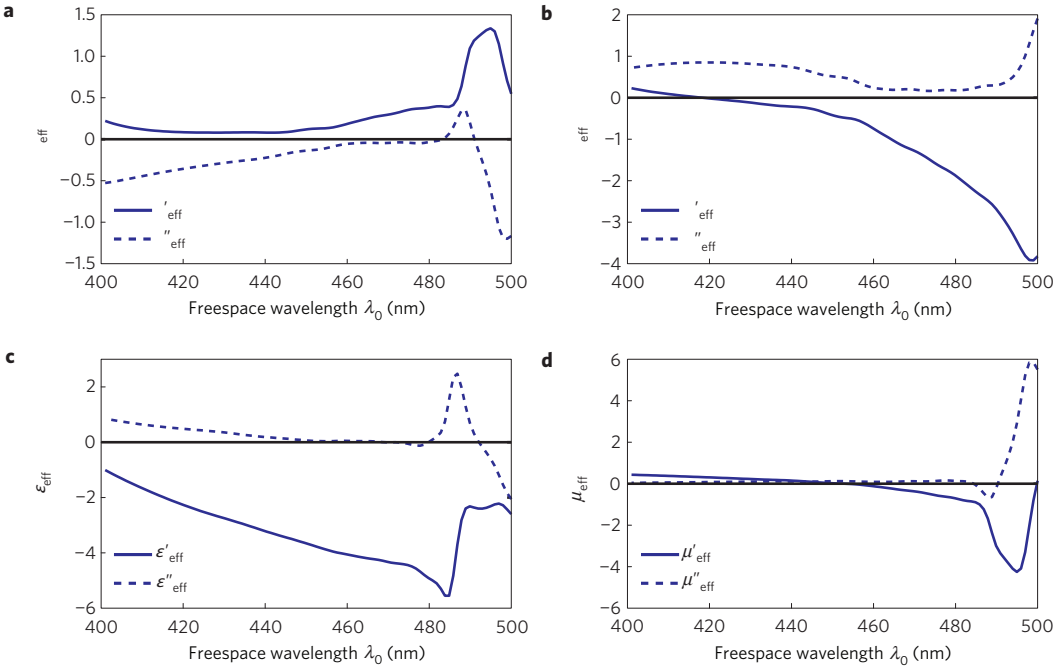

Figure 4 | NIM effective parameters. Effective parameters are calculated for a 100-nm-thick NIM slab excited at normal incidence over the 400–500 nm spectral range. **a**–**d**, The real (′) P (″) parts of the retrieve226(P)3effective relative impedance (**a**), index eff (**b**), relative permittivity ε_{eff} (**c**) relative permeability μ_{eff} (**d**).

incidence angles [18]. We note that simulations as in Fig. 3a show the semi-infinite NIM slab to reflect ~35% of the incident light, depending on angle, indicating that a

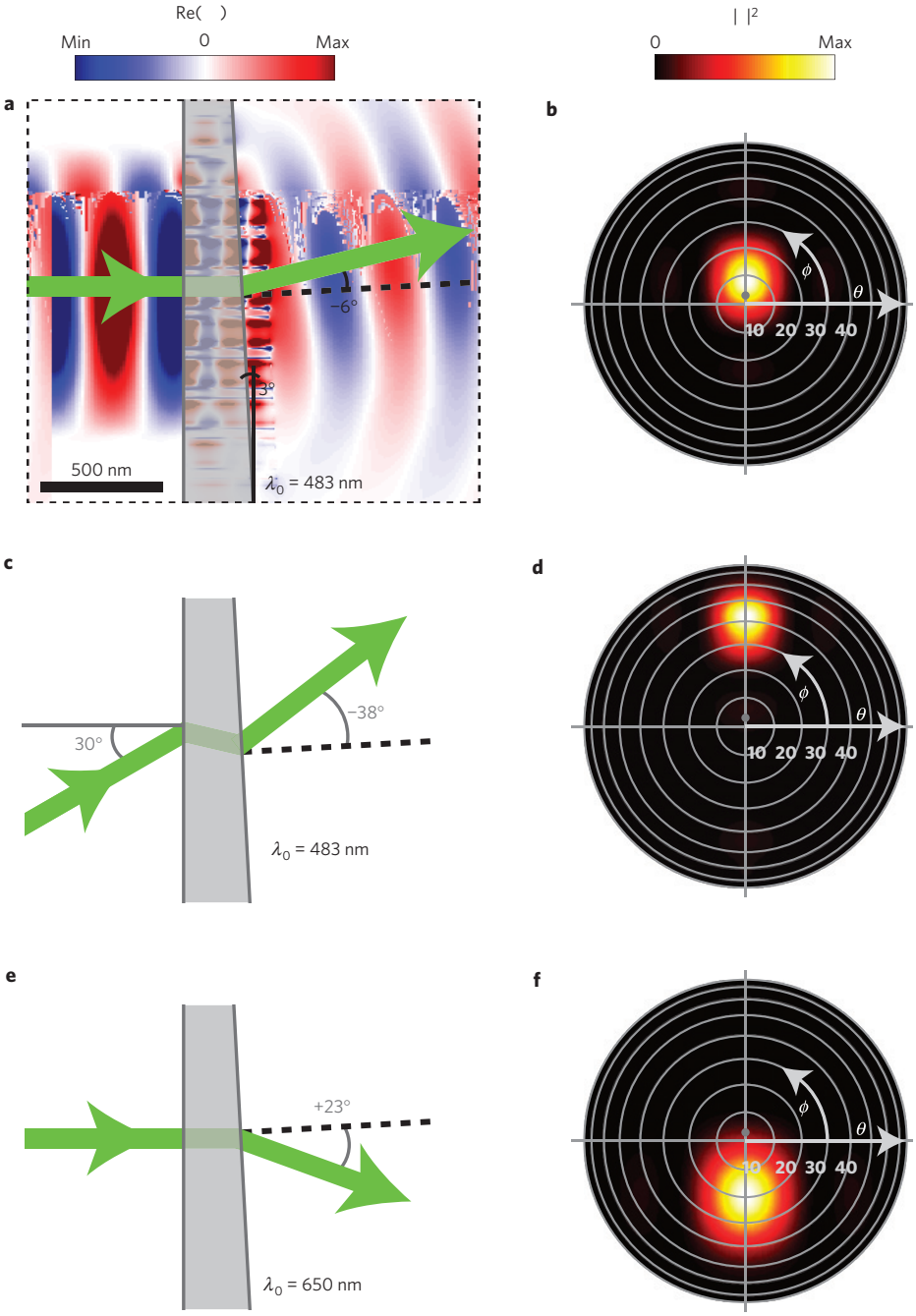

Figure 5 | Wedge refraction. a–f, A ~300-nm-thick metamaterial slab is illuminated from the left at normal (**a**,**b**,**e**,**f**) and 30° off-normal incidence (**c**,**d**). The right side of the slab is cut at a 3° angle to allow refraction (black dashed line indicates the surface normal). The wavelength of incident light is 483 nm (**a**–**d**) and 650 nm (**e**,**f**). The three panels on the left (**a**,**c**,**e**) depict the calculated power flow (green arrows), and the three corresponding right-side panels (**b**,**d**,**f**) show the steady-state electric field intensity in a polar plot, monitored at a distance of 10 μm behind the exit side of the slab. The output plane surface normal is indicated on the polar plots by a grey dot. In **a** we also plot the Re( ) field distribution along the plane of refraction.

angle of incidence. In that case, we cannot assign an effective materials index in terms of either power or phase, but rather assign a local effective mode index that is characteristic of an isolated waveguide mode.

However, as the array pitch is decreased, the waveguides begin to couple in such a way that both power and phase are able to propagate across the waveguide array. We find that coupling is easily achieved for the negative-index mode, because its strongly delocalized field distribution, which resides primarily in the metal, allows neighbouring structures to easily couple (see Fig. 2a insets and Supplementary Fig. S1). At a waveguide separation of roughly twice the mode skin depth of a single coaxial waveguide mode into the surrounding Ag, we find not only that power and phase are antiparallel, but also that they refract with an effective index close to the mode index of the constituent waveguides (Supplementary Fig. S3). By varying the incidence angle, the array response is found to be isotropic within a ±50° angular range (Supplementary Fig. S2).

This level of isotropy can be observed in Fig. 3b, which shows the constant-frequency surface formed by the wavevector **k** and Poynting vector **S** data derived from FDTD simulations. The figure clearly illustrates that both phase and power are antiparallel within

a ±50° range of incidence angles (corresponding to a ±20° angular range inside the material).

To confirm the validity of assigning an effective index to the coupled coaxial waveguide structure, we used FDTD to perform a parameter retrieval procedure[28,29] on a 100-nm-thick NIM slab (Fig. 1a) over the 400–500 nm spectral range. Figure 4 shows the resulting curves corresponding to the effective relative impedance z_{eff}, index n_{eff}, relative permittivity $\varepsilon_{\mathrm{eff}}$, and relative permeability μ_{eff} of the coupled coaxial NIM structure, with (′) and (″) denoting the parameters' real and imaginary parts, respectively. The extracted effective index curve (Fig. 4b) is found to closely resemble the mode index dispersion of a single coaxial waveguide structure (Fig. 2c) with n'_{eff} going from positive to negative values at $\lambda_0 \sim 420$ nm, with increasing wavelength. At $\lambda_0 = 483$ nm, we obtain a retrieved effective index of $n_{\mathrm{eff}} = -2.1 + i0.2$, corresponding to a FOM ∼ 10 that is consistent with the single coaxial waveguide FOM ∼ 8. For the retrieved effective relative permittivity $\varepsilon_{\mathrm{eff}}$ (Fig. 4c) we observe a material with $\varepsilon'_{\mathrm{eff}} < 0$ over the entire simulated spectral region, whereas for the effective relative permeability μ_{eff} (Fig. 4d) we get a material that is diamagnetic with $\mu'_{\mathrm{eff}} < 0$ over the 450–500 nm spectral range. Thus, we confirm that the coupled coaxial waveguide NIM structure has a double-negative index[21] composed of simultaneously negative real parts of the permittivity and permeability over the 450–500 nm spectral range.

To further corroborate our results, we have simulated the Snell–Descartes refraction of a ∼300-nm-thick wedged-shaped metamaterial slab cut at a 3° angle. Figure 5a depicts a time snapshot of the steady state Re(H_x) field distribution along the plane of refraction for $\lambda_0 = 483$ nm s-polarized light at normal incidence (Supplementary Movie S2). Figure 5a shows that light refracts negatively at the angled side of the prism, exiting the structure at an angle of −6° with respect to the surface normal. Figure 5b shows a polar plot of the refracted light projected into the far field. Using Snell's law and the observed negative refraction angle, we derive a refractive index for the metamaterial slab of $n_{\mathrm{eff}} = -1.8$, in agreement with the effective index derived from the observed wavevector inside the semi-infinite slab.

To demonstrate the insensitivity of the metamaterial-index to incidence angle, we also simulated the refraction of off-normal incident light through the 3° wedge. Figure 5c and d show the simulation results for $\lambda_0 = 483$ nm radiation incident at 30°. The green arrows in Fig. 5c indicate the direction of the Poynting vector for the incident and refracted beams. In this case the beam is refracted at an angle of −38° with respect to the surface normal, corresponding to an effective index $n_{\mathrm{eff}} = -2.2$, again consistent with the effective index found for the wedge excited at normal incidence. By varying the angle-of-incidence from normal incidence up to 50° for both s- and p-polarized light, we find consistent refractive indices ranging from −1.8 to −2.4. These data are summarized in Supplementary Fig. S2.

To illustrate the metamaterial's tunability with wavelength, we study the refraction of $\lambda_0 = 650$ nm radiation for which the mode index dispersion of a single waveguide element (Fig. 2a) shows a positive index ($n_{\mathrm{mode}} = 8.5$). Indeed, as Fig. 5e and f show, the beam is now refracted to the opposite side of the interface normal, at an angle of 23°, corresponding to a positive effective index of $n_{\mathrm{eff}} = 7.4$. We attribute the difference between the metamaterial effective index and isolated waveguide mode index to the possible excitation of higher-order waveguide modes. Thus, by illuminating the structure with frequencies either above or below the Ag/GaP surface plasmon resonance, we can excite both positive and negative refractive indices within the same metamaterial.

Realization of the metamaterial structure reported here involves the challenge of fabricating high-aspect-ratio nanoscale Ag channels. However, we have shown that 50-nm-wide coaxial apertures with aspect ratios >10 can readily be fabricated using focused ion beam milling[30]. For large-scale fabrication, a more tractable approach would be to use electron beam lithography in combination with high aspect ratio reactive ion etching. We also note that observation of the negative-index response requires only a modest total material thickness, that is, thick enough for a single waveguide to support the negative index waveguide mode. This can, for instance, be seen in our wedge simulations (for example, Fig. 5a) where the wedge thickness is only ∼300 nm and the material's negative index response is clearly observed. At $\lambda_0 = 483$ nm for an index of $n = -2$, a minimum thickness of ∼120 nm is required, corresponding to a modest coaxial channel aspect ratio of 4.

Methods

Coaxial waveguide dispersion relation. The dispersion relation of the constituent coaxial elements is calculated by solving Maxwell's equations in cylindrical coordinates[23,24] for a single MIM coaxial waveguide of infinite length. The azimuthal dependence of the electric and magnetic fields in the waveguide is described by the harmonic function $e^{in\psi}$ of order n. We consider only the modes with $n = 1$ as these are the lowest order linearly polarized modes that most strongly couple to free space radiation. The radial dependence of the fields in all three domains (metal–dielectric–metal) is described by solutions to the second order Bessel differential equation. We apply a Bessel function of the first kind J_n to the Ag core; a Hankel function of the first kind H_n to the Ag cladding; and a linear combination of both J_n and H_n functions to the dielectric channel. On each domain boundary we formulate four continuity conditions for the tangential components of the electric and magnetic fields. The optical eigenmodes of the coaxial waveguide are found when the determinant of the resulting homogeneous system of eight equations with eight unknown coefficients vanishes.

NIM slab refraction. For the semi-infinite metamaterial slab calculations, the NIM is modelled in FDTD (Lumerical FDTD Solutions 6.0) as a single unit cell (Fig. 1b) embedded in air with Bloch boundary conditions along the in-plane direction. The structure is excited with a continuous plane wave source incident at an angle θ. The appropriate electromagnetic fields are recorded to reconstruct the refraction of phase (Fig. 3a) along the plane of incidence. The refraction of power is obtained by spatially averaging the steady state Poynting vector components inside the material along the plane of incidence. The steady state electromagnetic fields are obtained by calculating the system's impulse response to a plane wave source with a Gaussian frequency spectrum centred at the frequency of interest.

Parameter retrieval. The parameter retrieval is calculated using FDTD by exciting a 100-nm-thick NIM slab embedded in air with a broadband plane wave source ranging from $\lambda_0 = 400$ to 500 nm at normal incidence. The steady state field distributions are recorded, and the complex reflection r and transmission t coefficients are calculated by taking the ratios $r = E_r/E_0$ and $t = E_t/E_0$, where E_0 is the electric field amplitude of the incident wave and E_r and E_t are the reflected and transmitted electric field amplitudes, respectively. Standard inverted reflection and transmission parameter equations found in literature[28,29] are used to relate r and t to the layer's effective impedance z_{eff} and index n_{eff}. The effective permittivity $\varepsilon_{\mathrm{eff}}$ and permeability μ_{eff} are calculated through the relations $\varepsilon = n/z$ and $\mu = nz$.

Wedge refraction. For the wedge refraction simulations, the NIM wedge is modelled in FDTD as a ∼300-nm-thick metamaterial-slab cut at a 3° angle. The structure is excited with a continuous wave source centred at the desired excitation frequency using a ∼1-μm-wide hollow metallic waveguide oriented perpendicular to the metamaterial's input plane. The appropriate electromagnetic fields are recorded to reconstruct the refraction of phase (Fig. 5a) along the plane of incidence. The structure is also excited from free space with a ∼1.5 μm spot size Gaussian beam. Using the steady state field distribution at the output side of the wedge, a near-to-far-field transformation is performed to determine the refracted-beam profile at a distance of 10 μm behind the exit side of the structure.

Received 28 October 2009; accepted 15 March 2010; published online 18 April 2010

References

1. Pendry, J. B. Negative refraction makes a perfect lens. *Phys. Rev. Lett.* **85,** 3966–3969 (2000).
2. Fang, N., Lee, H., Sun, C. & Zhang, X. Sub-diffraction-limited optical imaging with a silver superlens. *Science* **308,** 534–537 (2005).
3. Alu, A. & Engheta, N. Multifrequency optical invisibility cloak with layered plasmonic shells. *Phys. Rev. Lett.* **100,** 113901 (2008).
4. Cai, W., Chettiar, U. K., Kildishev, A. V. & Shalaev, V. M. Optical cloaking with metamaterials. *Nature Photon.* **1,** 224–227 (2007).
5. Liu, R. *et al.* Broadband ground-plane cloak. *Science* **323,** 366–369 (2009).

6. Pendry, J. B., Schurig, D. & Smith, D. R. Controlling electromagnetic fields. *Science* **312,** 1780–1782 (2006).
7. Parazzoli, C. G. *et al.* Experimental verification and simulation of negative index of refraction using Snell's law. *Phys. Rev. Lett.* **90,** 107401 (2003).
8. Shelby, R. A., Smith, D. R. & Schultz, S. Experimental verification of a negative index of refraction. *Science* **292,** 77–79 (2001).
9. Dolling, G. *et al.* Simultaneous negative phase and group velocity of light in a metamaterial. *Science* **312,** 892–894 (2006).
10. Dolling, G., Wegener, M. & Linden, S. Realization of a three-functional-layer negative-index photonic metamaterial. *Opt. Lett.* **32,** 551–553 (2007).
11. Shalaev, V. M. *et al.* Negative index of refraction in optical metamaterials. *Opt. Lett.* **30,** 3356–3358 (2005).
12. Valentine, J. *et al.* Three-dimensional optical metamaterial with a negative refractive index. *Nature* **455,** 376–379 (2008).
13. Zhang, S. *et al.* Experimental demonstration of near-infrared negative-index metamaterials. *Phys. Rev. Lett.* **95,** 137404 (2005).
14. Dolling, G., Wegener, M., Soukoulis, C. M. & Linden, S. Negative-index metamaterial at 780 nm wavelength. *Opt. Lett.* **32,** 53–55 (2007).
15. Veselago, V. G. The electrodynamics of substances with simultaneously negative values of ε and μ. *Sov. Phys. Usp.* **10,** 509–514 (1968).
16. Pendry, J. B., Holden, A. J., Robbins, D. J. & Stewart, W. J. Magnetism from conductors and enhanced nonlinear phenomena. *IEEE Trans. Microw. Theory* **47,** 2075–2084 (1999).
17. Smith, D. R. *et al.* Composite medium with simultaneously negative permeability and permittivity. *Phys. Rev. Lett.* **84,** 4184–4187 (2000).
18. Dionne, J. A., Verhagen, E., Polman, A. & Atwater, H. A. Are negative index materials achievable with surface plasmon waveguides? A case study of three plasmonic geometries. *Opt. Express* **16,** 19001–19017 (2008).
19. Lezec, H. J., Dionne, J. A. & Atwater, H. A. Negative refraction at visible frequencies. *Science* **316,** 430–432 (2007).
20. Shvets, G. Photonic approach to making a material with a negative index of refraction. *Phys. Rev. B* **67,** 035109 (2003).
21. Chettiar, U. K. *et al.* Dual-band negative index metamaterial: Double negative at 813 nm and single negative at 772 nm. *Opt. Lett.* **32,** 1671–1673 (2007).
22. Liu, Y., Bartal, G. & Zhang, X. All-angle negative refraction and imaging in a bulk medium made of metallic nanowires in the visible region. *Opt. Express* **16,** 15439–15448 (2008).
23. Baida, F. I., Belkhir, A., Labeke, D. V. & Lamrous, O. Subwavelength metallic coaxial waveguides in the optical range: Role of the plasmonic modes. *Phys. Rev. B* **74,** 205419 (2006).
24. Novotny, L. & Hafner, C. Light propagation in a cylindrical waveguide with a complex, metallic, dielectric function. *Phys. Rev. E* **50,** 4094–4106 (1994).
25. Johnson, P. B. & Christy, R. W. Optical constants of the noble metals. *Phys. Rev. B* **6,** 4370–4379 (1972).
26. Palik, E. D. & Ghosh, G. *Handbook of Optical Constants of Solids* (Academic, 1985).
27. Soukoulis, C. M., Linden, S. & Wegener, M. Negative refractive index at optical wavelengths. *Science* **315,** 47–49 (2007).
28. Smith, D. R., Vier, D. C., Koschny, T. & Soukoulis, C. M. Electromagnetic parameter retrieval from inhomogeneous metamaterials. *Phys. Rev. E* **71,** 036617 (2005).
29. Minowa, Y. *et al.* Evaluation of effective electric permittivity and magnetic permeability in metamaterial slabs by terahertz time-domain spectroscopy. *Opt. Express* **16,** 4785–4796 (2008).
30. de Waele, R., Burgos, S. P., Polman, A. & Atwater, H. A. Plasmon dispersion in coaxial waveguides from single-cavity optical transmission measurements. *Nano Lett.* **9,** 2832–2837 (2009).

Acknowledgements

We would like to thank J. A. Dionne, H. J. Lezec, E. Verhagen, and A. F. Koenderink for fruitful discussions. This work was supported by the Energy Frontier Research Center program of the Office of Science of the Department of Energy under grant DE-SC0001293, by the National Science Foundation under the Graduate Research Fellowship Program, and made use of facilities supported by the Center for Science and Engineering of Materials, an NSF Materials Research Science and Engineering Center at Caltech. This work is also part of the research program of the 'Stichting voor Fundamenteel Onderzoek der Materie (FOM)', which is financially supported by the 'Nederlandse Organisatie voor Wetenschappelijk Onderzoek (NWO)'. It was also supported by 'NanoNed', a nanotechnology program funded by the Dutch Ministry of Economic Affairs.

Author contributions

H.A.A. conceived the idea. H.A.A. and A.P. provided guidance throughout the project's development. S.P.B. took the lead in the FDTD analysis. R.D.W. took the lead in developing the analytic coaxial waveguide theory and code. S.P.B., R.D.W., A.P. and H.A.A. all contributed to the writing and editing of the manuscript.

Additional information

The authors declare no competing financial interests. Supplementary information accompanies this paper on www.nature.com/naturematerials. Reprints and permissions information is available online at http://npg.nature.com/reprintsandpermissions. Correspondence and requests for materials should be addressed to H.A.A.